Monthly Notices
of the
ROYAL ASTRONOMICAL SOCIETY

MNRAS **466,** 4568–4572 (2017)
Advance Access publication 2016 December 17

doi:10.1093/mnras/stw3287

A quasar discovered at redshift 6.6 from Pan-STARRS1

Ji-Jia Tang,[1,2]★ Tomotsugu Goto,[3]★ Youichi Ohyama,[2]★ Wen-Ping Chen,[4] Fabian Walter,[5] Bram Venemans,[5] Kenneth C. Chambers,[6] Eduardo Bañados,[7]† Roberto Decarli,[5] Xiaohui Fan,[8] Emanuele Farina,[5] Chiara Mazzucchelli,[5] Nick Kaiser[6] and Eugene A. Magnier[6]

[1]*Graduate Institute of Astrophysics, National Taiwan University, No.1 Section 4 Roosevelt Rd., Taipei 10617, Taiwan*
[2]*Institute of Astronomy and Astrophysics, Academia Sinica, No.1, Section 4, Roosevelt Rd., Taipei 10617, Taiwan*
[3]*Institute of Astronomy, National Tsing Hua University, 101, Section 2, Kuang Fu Rd., Hsinchu 30013, Taiwan*
[4]*Graduate Institute of Astronomy, National Central University, No. 300, Zhongda Rd., Zhongli Dist., Taoyuan City 32001, Taiwan*
[5]*Max-Plank Institute for Astronomy, Königstuhl 17, D-69117 Heidelberg, Germany*
[6]*Institute for Astronomy, University of Hawaii at Manoa, Honolulu, HI 96822, USA*
[7]*Carnegie Observatories, 813 Santa Barbara Street, Pasadena, CA 91101 USA*
[8]*Steward Observatory, University of Arizona, Tucson, AZ 85721, USA*

Accepted 2016 December 14. Received 2016 December 13; in original form 2016 September 20

ABSTRACT

Luminous high-redshift quasars can be used to probe of the intergalactic medium in the early universe because their UV light is absorbed by the neutral hydrogen along the line of sight. They help us to measure the neutral hydrogen fraction of the high-z universe, shedding light on the end of reionization epoch. In this paper, we present a discovery of a new quasar (PSO J006.1240+39.2219) at redshift $z = 6.61 \pm 0.02$ from Panoramic Survey Telescope & Rapid Response System 1. Including this quasar, there are nine quasars above $z > 6.5$ up to date. The estimated continuum brightness is $M_{1450} = -25.96 \pm 0.08$. PSO J006.1240+39.2219 has a strong Ly α emission compared with typical low-redshift quasars, but the measured near-zone region size is $R_{\rm NZ} = 3.2 \pm 1.1$ proper megaparsecs, which is consistent with other quasars at $z \sim 6$.

Key words: quasars: general – quasars: individual – dark ages, reionization, first stars.

1 INTRODUCTION

Quasars or quasi-stellar objects (QSOs) are supermassive black holes (SMBHs) with accretion discs in the centre of a galaxy. They are amongst the most luminous observable objects after the epoch of recombination at $z \sim 1100$. High-redshift ($z \geq 6.0$) quasars are, thus, a powerful tool to probe the early universe. A quasar's spectrum can be used to estimate the mass of SMBH (e.g. Mortlock et al. 2011; Morganson et al. 2012; De Rosa et al. 2014; Venemans et al. 2015), which constrains the evolution and formation model of SMBH within a time-scale of <1 Gyr (Li et al. 2007; Tanaka & Haiman 2009). The Gunn–Peterson (GP) (Gunn & Peterson 1965) troughs in the spectrum can constrain the neutral hydrogen (H I) fraction in the early universe (Becker et al. 2001; Fan et al. 2002; Fan 2006; Goto 2006; Bolton et al. 2011; Goto et al. 2011). The GP troughs observed in the $z \sim 6$ quasars discovered by Sloan Digital Sky Survey (Fan et al. 2006; McGreer et al. 2006) suggest that the reionization epoch of the universe ends around $z \sim 6$.

High-redshift quasars can be found by a red colour, between two adjacent broad-bands caused by the strong intergalactic medium (IGM) absorption on the blue side of the redshifted Ly α emission (1216 Å at rest frame). The number of quasars we can find is limited by the survey area and depth. After decades of searching, more than 100 quasars are found in the range $5.7 < z < 6.5$ from various kind of surveys (e.g. Bañados et al. 2016; Mortlock 2016). Most of them are i-dropouts that are very red in $i - z$ colour. To search for quasar above $z > 6.5$, z-dropouts are needed because the Ly α line is redshifted to wavelength $\lambda \geq 9000$ Å. Several surveys covering wavelength ∼1 μm have been dedicated to search for them and only eight are found in previous work. The highest redshift quasar at $z = 7.085$ was found by Mortlock et al. (2011) using UK infrared Telescope Infrared Deep Sky Survey (Lawrence et al. (2007)). Venemans et al. (2013) discovered three quasars above $z > 6.5$ using Visible and Infrared Survey Telescope for Astronomy Kilo-degree Infrared Galaxy survey, while Venemans et al. (2015) found another three in the range $6.5 < z < 6.7$ using the Panoramic Survey Telescope & Rapid Response System 1

★ E-mail: jjtang@asiaa.sinica.edu.tw (J-JT); tomo@phys.nthu.edu.tw (TG); ohyama@asiaa.sinica.edu.tw (YO)
† Carnegie-Princeton Fellow.

(Pan-STARRS1 or PS1; Kaiser et al. 2002, 2010). The *Subaru* High-z Exploration of Low-Luminosity Quasars (SHELLQs) survey also discovered one quasar/galaxy at $z \sim 6.8$ (Matsuoka et al. 2016) However, the redshift of this QSO is uncertain due to the absence of strong emission lines.

In this paper, we report a discovery of a new quasar at $z = 6.6$ selected from PS1 with a spectroscopic confirmation. This is the seventh highest quasar among nine z-dropout quasar ($z > 6.5$) known to date.

We adopt a cosmology with $\Omega_M = 0.28$, $\Omega_b = 0.045$, $\Omega_\Lambda = 0.72$ and $H_0 = 70\,\mathrm{km\,s^{-1}\,Mpc^{-1}}$ (Komatsu et al. 2011). All magnitudes are given in the AB system.

2 CANDIDATE SELECTION

PS1 covers more than 30 000 deg^2 with five imaging filters (g_{P1}, r_{P1}, i_{P1}, z_{P1}, y_{P1}; Stubbs et al. 2010; Tonry et al. 2012). We have selected our QSO targets from PS1 (version PV2) as follows. At $z > 6.5$, QSOs are the z-dropouts. As the Ly α line moves to the y band, thus QSOs have red $z - y$ colour and are very faint or undetectable in the z and bluer bands. At first, we selected point sources as objects with a small difference between Kron and point spread function (PSF) magnitudes ($-0.3 < y_{kron} - y_{psf} < 0.3$) from the PS1 multiepoch stack data. Further we require a very red colour of $z - y > 2.0$ and signal to noise ratio (SNR) larger than 10 in the y band. Similar criteria were used by Venemans et al. (2015) who recently reported a discovery of theee new $z > 6.5$ QSOs from PS1. We also require our candidates to have >24 mag in the i and z bands that correspond to the brightness of the sky background in PS1. This criterion is to select candidates below detection limits of PS1 in the i and z bands.

To exclude spurious dropouts as a result of transient or moving single-epoch objects, we require that all of our candidates are observed and detected at least on two different dates. This ensures that each of our candidates is a real object.

Among the objects that satisfied the criteria above, we have put priority on those with good visibility at the time of the observation, brighter y-band magnitude and redder $z - y$ colour. The remaining candidates selected in this way are visually examined using the single epoch PS1 images. Many of them are rejected by eye as they are obvious spurious or contaminated by a nearby bright star. This eye-rejection process is not automated nor well controlled. As a result, our selection procedure is heterogeneous and would not be able to yield a statistically characterizable quasar sample. It is important future work to establish a more controlled process based on a newer release of the PS1 catalogue. We further check our candidates with *Wide-field Infrared Survey Explorer* catalogue (*WISE*; Wright et al. 2010), but they are not detected in the ALLWISE catalogue, due to the faintness of our candidates.

3 FOLLOW-UP SPECTROSCOPY AND DATA REDUCTION

The spectroscopic observation was carried out with the Subaru Faint Object Camera and Spectrograph (Kashikawa et al. 2002) on 2015 November 2. The weather was good and the seeing size was 0.75 arcsec. We used the VPH900 grating with O58 order cut filter with 2×2 binning, which gave us a wavelength coverage between 7434 and 10582 Å and a pixel resolution of 1.48 Å. We used a 0.8 arcsec long slit, with a spectroscopic resolution of $R \sim 600$. We observed 12 candidates with the first exposure of 1000 s. After the first exposure, if the target did not have an emission line to be a quasar, we moved on to the next target. Most contaminating objects were late-type stars. During the process, PSO J006.1240+39.2219 turned out to be a high-redshift quasar, noticed by a strong Ly α emission line. Therefore, we took five exposures with 1000 s each for this target. Each exposure was taken at a different position on the chip to correct for systematic effects. We also observed BD+28D4211 as a standard star for 30 s.

For the data reduction, we follow the standard IRAF routines. We begin with flat fielding. The dome flat was taken for 2 s, and we correct for vignetting and the absorption due to the coating inside the dome. After normalized for the corrected flat fielding, we perform a wavelength calibration. We identify sky lines for five exposures independently and fit them into the same wavelength range (7434–10582 Å) so that we can combine them without further wavelength transformation between different exposures later. We perform first order sky background subtraction using only 60 pixels in total around the quasar position in the spatial direction. After trials and errors, this gives us the best subtraction result. After sky background subtraction for five exposures, we combine them using 3σ robust mean. We use APALL task in IRAF to derive 1D spectrum from 2D images. However, we need the trace from the standard star because the target is very faint blueward of Ly α emission. We apply the same flat fielding and wavelength calibration to the standard star, trace the spectrum using APALL and apply it for the quasar. Thus, we have an accurate trace bluer than redshifted Ly α emission, where we can measure the absorption.

To convert counts into flux, we use the sensitivity function derived from the standard star to correct for the wavelength-dependent feature. Then, we scale the spectrum flux to the extinction-corrected ($A_y = 0.08$) PS1 magnitude of $y = 20.00$, which is 70 percent of the spectrum flux we calibrate above. By fitting the PSF on the spatial direction of the 2D image, we estimate that the slit loss of standard star to that of the target is 80 percent, which is comparable to the 70 percent we scale above. The spectrum error is derived from the count dispersion between five exposures by assuming the pixel performance is the same for different exposures. We remove those pixels whose value is more than 3σ away from the mean of five exposures to eliminate cosmic ray. Then divide the value by the square root of the number of frames left. After considering error propagation, we turn the error into flux unit. This flux error is used for lines and continuum fitting, and transmission calculation in Section 4. The resulting spectrum and the 1σ spectrum error is presented in Fig. 1.

4 DATA ANALYSIS AND RESULTS

In our spectrum, three emission lines, Ly α, N V and O I+Si II, are detected. The equivalent widths (EWs) are calculated using the wavelength ranges in Vanden Berk et al. (2001). We also integrate the same wavelength range to obtain the luminosity and the flux after subtracting the power-law continuum. The fitting procedures for Ly α, N V, O I+Si II and the continuum are described in Sections 4.3, 4.1, 4.2 and 4.2, respectively. We estimate the luminosities of these emission lines in Table 1.

4.1 Redshift

To measure the redshift, since Ly α may be partially absorbed, we use N V line (hereafter $z_{N\,V}$), which is a doublet line at λ 1238.82 and 1242.81 Å. By using a least-squares fitting to fit a double Gaussian with same width plus linear continuum, we derive the redshift of PSO J006.1240+39.2219, which is 6.61 ± 0.02 (Table 2). We find a linear continuum is good enough because the fitting wavelength

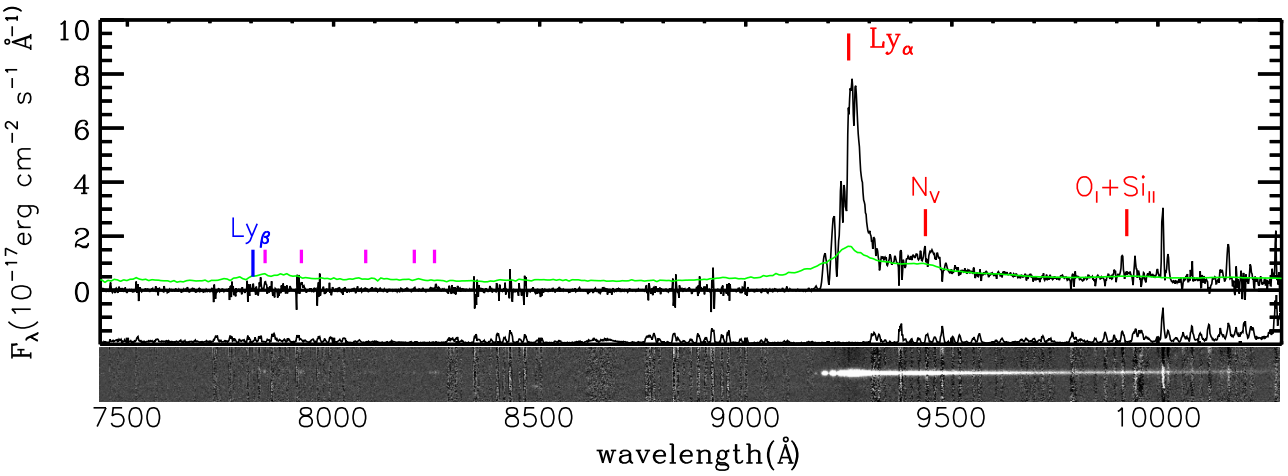

Figure 1. The spectrum of PSO J006.1240+39.2219. The spectrum and spectrum error are combined into upper and lower panels, respectively. The spectrum error is scaled to two times larger for clarity. The green line is the redshifted composite quasar spectrum from Vanden Berk et al. (2001) scaled to the continuum flux of J006.1240+39.2219. Three detected lines, Ly α, N V and O I+Si II are marked in red. Ly β, which is marked in blue, is not detected. Note that there are faint detections at 7834, 7922, 8078, 8196 and 8245 Å, which are shown in magenta. The two-dimensional spectrum is also shown here for comparison.

Table 1. *The luminosities of the emission lines of PSO J006.1240+39.2219.*

Line	Luminosity (10^{44} erg s^{-1})
Ly α	17.0 ± 0.1
N V	4.9 ± 0.1
O I+Si II	2.0 ± 0.1

http://wise2.ipac.caltech.edu/docs/release/allwise/expsup/sec2_3a.html

Table 2. The basic properties of J006.1240+39.2219.

	J006.1240+39.2219
RA(J2000)	$00^h24^m29.77^s$
Dec.(J2000)	$39^\circ13'18.95''$
$z_{P1,\,PSF}$	25.15 ± 2.98^a
$y_{P1,\,PSF}$	20.08 ± 0.08
$W1_{5\sigma}$	$>20.5^b$
$W2_{5\sigma}$	$>19.7^b$
N V redshift ($z_{N\,V}$)	6.61 ± 0.02
$M_{1450}{}^c$	-25.96 ± 0.08
$M_{1450}{}^d$	-25.94 ± 0.08
R_{NZ} (Mpc)	3.2 ± 1.1
$R_{NZ,corr}$ (Mpc)	4.3 ± 1.5

Notes. [a]The value is the output from PS1 PV2 data base, which is much fainter than the detection z-band limit of PS1 (21.6; Morganson et al. 2012). Therefore, it is untrustworthy.
[b]The SNR 5 sensitivity limit.[1]
We adopt Table 1 in the website and check the magnitude of the closest patch to our quasar, then convert it to AB magnitude. There is actually one ALLWISE detection 7.6 arcsec away from our quasar, which may be a combination of this quasar and the other nearby source due to the low spatial resolution of *WISE*.
[c]Assume $f_\lambda \propto \lambda^{-1.5}$ (Fan et al. 2003).
[d]Assume $f_\lambda \propto \lambda^{-1.7}$ (Selsing et al. 2016).

range is narrow. The actual redshift may be influenced by the broad-line property of N V, which causes about 0.02 of redshift error. In Fig. 1, we overplot the redshifted composite quasar spectrum from Vanden Berk et al. (2001). The spectral resolution is adjusted to match for a fair comparison. This shows that Ly α emission of PSO J006.1240+39.2219 is much stronger than those quasars at low redshifts. This is the seventh highest redshift quasar known to date (Section 1).

4.2 M_{1450}

Conventionally, previous work used the absolute magnitude at rest-frame 1450 Å (M_{1450}) to represent the quasar continuum (e.g. Bañados et al. 2014; Mortlock et al. 2011; Venemans et al. 2015). The M_{1450} of PSO J006.1240+39.2219 can be derived from measuring the flux at $1450 \times (z + 1)$ Å. However, because the redshifted 1450 Å of PSO J006.1240+39.2219 is 11032.9 Å, we extrapolate the continuum to estimate the flux. We attempt two different continuum shapes, $f_\lambda \propto \lambda^{-1.5}$ (Fan et al. 2003) and $f_\lambda \propto \lambda^{-1.7}$ (Selsing et al. 2016), to fit the wavelength interval between 9750 and 10200 Å. We also consider the O I+Si II lines located inside this interval. We fit the power-law continuum plus a double Gaussian (O I+Si II) with least-squares fitting. Therefore, the estimated M_{1450} of PSO J006.1240+39.2219 are -25.96 ± 0.08 for -1.5 power law and -25.94 ± 0.08 for -1.7 power law (Table 2), which is similar to other quasars at $z > 6.5$ (Venemans et al. 2015). The error of M_{1450} is dominated by the y-band magnitude error in PS1.

4.3 Optical depth and near zone region

To determine GP effective optical depth τ_{GP}^{eff}, we need a good estimate of the original continuum before absorption. We cannot use the composite spectrum from low-redshift quasars (Vanden Berk et al. 2001) because PSO J006.1240+39.2219 has much stronger Ly α emission. We find a single Gaussian is not suitable because there is a much broader tail of Ly α emission. Therefore, we fit the Ly α feature with a double Gaussian at 1215.67 Å

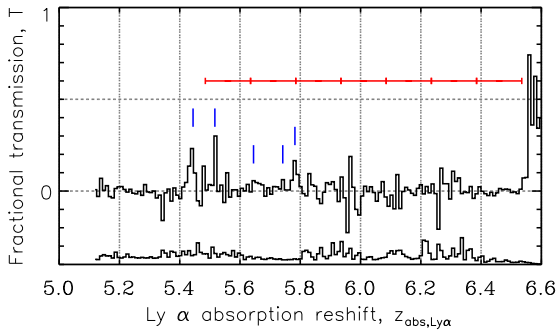

Figure 2. The T–z diagram. This shows the transmission and the transmission error below redshifted Ly α emission in terms of the Ly α absorption redshift. They are binned by a factor of 8 pixels for clarification. There are five Ly α absorption residuals labeled in the blue short vertical line. The spectra shown is used to derive the effective optical depth of GP effect. The red horizontal line with nodes shows the bins of optical depth used in Table 3.

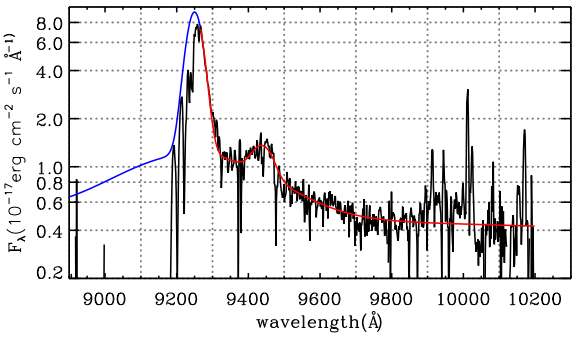

Figure 3. The simultaneous fitting of Ly α, N v and continuum. The red line is the region for fitting and the blue line is extrapolation. This fitting is used for the transmission calculation. The fitting method is described in Section 4.3.

(Vanden Berk et al. 2001) but with different widths with the fixed redshift at $z_{\rm N\,V}$. A similar method is used by Zhang et al. (2015).

We derive GP optical depth from the weighted transmission, T, in a redshift range of $5.56 < z < 6.46$ to avoid both Ly α and Ly β emission. The transmission (Fig. 2) are measured by dividing the observed spectrum by the best-fitting continuum, which includes Ly α double Gaussian, N v double Gaussian and the continuum power-law as shown in Fig. 3. Then we bin the transmission within $\Delta z = 0.15$ by considering the squared transmission error $\sigma_{\rm T}^2$ as a variance to derive weighted average transmission. We calculate the weighted transmission error by squared root of the reciprocal of the $\Sigma(1/\sigma_{\rm T}^2)$ in the bin. However, this error may be underestimated due to noise correlations between contiguous pixels (e.g. pixels affected by a strong sky line). Finally, we use $\tau_{\rm GP}^{\rm eff} = -\ln(T)$ to calculate GP optical depth (Fan et al. 2006). The lower limit of the GP optical depth may be lower due to the noise correlation. The result is shown in Table 3 and Fig. 4.

We calculate the weighted transmission of Ly β in the wavelength below rest-frame 1017 Å, considering, at the same time, the Ly α absorption at the same wavelength based on the equation 5 in Fan et al. (2006). The weighted transmission error of Ly β is determined by both the uncertainty of Ly α absorption equation and the observed spectrum error, where the former error dominates. After obtaining τ_β from the transmission, we apply the $\tau_\alpha/\tau_\beta = 2.25$ from the discussion in Fan et al. (2006) to derive τ_α for Ly β optical depth. The results are shown in Table 3 and Fig. 4.

Table 3. The transmission and the GP optical depth. This shows the weighted transmission and effective optical depth of binned redshift interval for Ly α and Ly β. Both transmission and optical depth error are in 2σ error if not specified. Those three bins in Ly α that show positive transmission after considering errors are caused by the faint detections in Fig. 1.

Redshift	Line	Transmission	τ_α
6.46	Ly α	-0.004 ± 0.006	>6.6
6.31	Ly α	0.007 ± 0.011	>4.0
6.16	Ly α	-0.010 ± 0.016	>5.3
6.01	Ly α	-0.022 ± 0.012	>6.2[a]
5.86	Ly α	0.032 ± 0.013	$3.4^{+0.5}_{-0.4}$
5.71	Ly α	0.027 ± 0.010	$3.6^{+0.5}_{-0.3}$
5.56	Ly α	0.020 ± 0.014	$3.9^{+1.3}_{-0.5}$
6.46	Ly β	-0.085 ± 0.146	>6.1
6.31	Ly β	-0.010 ± 0.120	>4.8

Note. [a]Since the transmission is too negative, we have to use 4σ limit to show the optical depth.

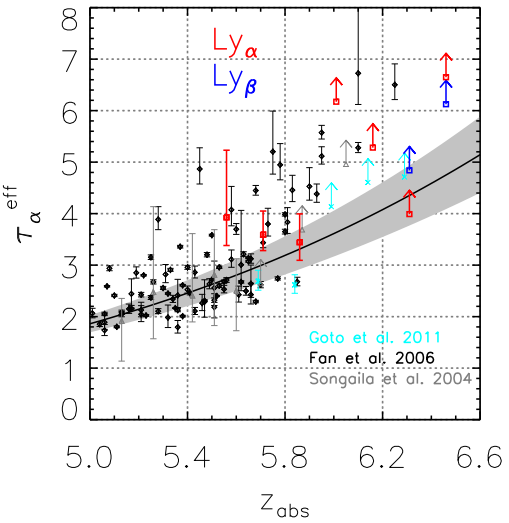

Figure 4. The GP optical depth from the spectrum of PSO J006.1240+39.2219. This shows the comparison of GP optical depth between PSO J006.1240+39.2219 and previous work. We adopt the values from Table 3 to show the optical depth from both Ly α (red) and Ly β (blue) absorption. The lower limit of the GP optical depth may be lower due to the noise correlation between contiguous pixels. The cyan crosses with error bars show the value in Goto et al. (2011) and the 2σ lower limit is used for non-detection. The black diamonds and grey triangles with error bars are the $\tau_\alpha^{\rm eff}$ in Fan et al. (2006) and Songaila (2004), respectively. The solid curve with shaded region shows the best-fitting power law with the error for Ly α absorption at $z_{\rm abs} < 5.5$:$\tau_\alpha^{\rm eff} = (0.85 \pm 0.06)[(1+z)/5]^{(4.3\pm0.3)}$ (Fan et al. 2006).

We follow the following equation of Carilli et al. (2010) to calculate near-zone region size $R_{\rm NZ}$.

$$R_{\rm p,NZ} = (D_{\rm Q} - D_{\rm GP})/(1 + z_{\rm Q}). \quad (1)$$

The $D_{\rm Q}$ and $D_{\rm GP}$ are the comoving distances of the redshift of the quasar host galaxy ($z_{\rm Q}$) and the redshift where the transmission drops below 0.1 ($z_{\rm GP}$), respectively. We present the proper distance $R_{\rm p}$–T diagram in Fig. 5. The transmission is smoothed to 20 Å. The near-zone region $R_{\rm NZ}$ is defined by the $R_{\rm p}$ where $T \sim 0.1$. To reduce the effect of different luminosity, we correct the near-zone region by $R_{\rm NZ,corr} = 10^{0.4\times(27+M_{1450,\rm AB})/3} R_{\rm NZ}$ (Fan et al. 2006). We measure

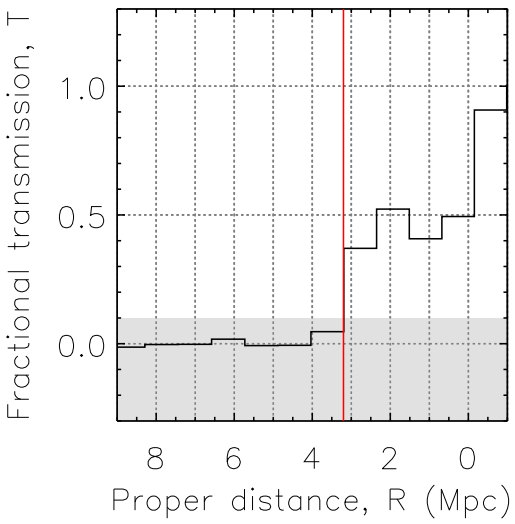

Figure 5. The T–$R_{\rm p}$ diagram. This shows the transmission that is smoothed for 20 Å, redshifted below Ly α emission in terms of the proper distance $R_{\rm p}$. The red line shows $R_{\rm NZ}$. The error of $R_{\rm NZ}$ is estimated by the uncertainty of redshift $z_{\rm N\,V}$.

$R_{\rm NZ} = 3.2 \pm 1.1$ (Mpc) and $R_{\rm NZ,corr} = 4.3 \pm 1.5$ (Mpc) (Table 2). The error of $R_{\rm NZ}$ are calculated from the error propagation of equation (1) assuming $\Delta_{z_{\rm Q}} = 0.02$ and $\Delta_{z_{\rm GP}} = 0.01$ (Carilli et al. 2010). The near-zone region of PSO J006.1240+39.2219 is consistent with other comparably distant quasars, although it has much stronger Ly α.

5 SUMMARY

We discovered a new quasar PSO J006.1240+39.2219 at $z = 6.61 \pm 0.02$, which is the seventh highest redshift quasar known to date. The number of z-dropout ($z > 6.5$) quasars reaches nineafter the discovery of PSO J006.1240+39.2219. The rest-frame UV luminosity $M_{1450} = -25.96 \pm 0.08$ (-25.94 ± 0.08) is comparable to other z-dropout quasars, but the Ly α emission is much stronger than typical quasars obtained from low redshift (Vanden Berk et al. 2001). The $R_{\rm NZ,corr} = 4.3 \pm 1.5$ (Mpc) of PSO J006.1240+39.2219 follows the trend $R_{\rm NZ,corrected} = (7.2 \pm 0.2) - (6.1 \pm 0.7) \times (z - 6)$ derived from Venemans et al. (2015).

ACKNOWLEDGEMENTS

We thank the anonymous referee for many insightful comments. We acknowlege L.Cowie for useful discussion. The Pan-STARRS1 Surveys (PS1) have been made possible through contributions by the Institute for Astronomy, the University of Hawaii, the Pan-STARRS Project Office, the Max-Planck Society and its participating institutes, the Max Planck Institute for Astronomy, Heidelberg and the Max Planck Institute for Extraterrestrial Physics, Garching, The Johns Hopkins University, Durham University, the University of Edinburgh, the Queen's University Belfast, the Harvard-Smithsonian Center for Astrophysics, the Las Cumbres Observatory Global Telescope Network Incorporated, the National Central University of Taiwan, the Space Telescope Science Institute, and the National Aeronautics and Space Administration under Grant No. NNX08AR22G issued through the Planetary Science Division of the NASA Science Mission Directorate, the National Science Foundation Grant No. AST-1238877, the University of Maryland, Eotvos Lorand University (ELTE), and the Los Alamos National Laboratory. TG acknowledges the support by the Ministry of Science and Technology (MoST) of Taiwan through grant National Science Council (NSC) 103-2112-M-007-002-MY3 and 105-2112-M-007-003-MY3, and Youichi Ohyama acknowledges the support by the MoST of Taiwan through grant NSC 100-2112-M-001-001-MY3, 104-2112-M-001-034- and 105-2112-M-001-024-. We thank Dr Ekaterina Koptelova for the assistance in the observation.

REFERENCES

Bañados E. et al., 2014, AJ, 148, 14
Bañados E. et al., 2016, ApJS, 227, 11
Becker R. H. et al., 2001, AJ, 122, 2850
Bolton J. S. et al., 2011, MNRAS, 416, L70
Carilli C. L. et al., 2010, ApJ, 714, 834
De Rosa G. et al., 2014, ApJ, 790, 145
Fan X., 2006, New Astron. Rev., 50, 665
Fan X., Narayanan V. K., Strauss M. A., White R. L., Becker R. H., Pentericci L., Rix H.-W., 2002, AJ, 123, 1247
Fan X. et al., 2003, AJ, 125, 1649
Fan X. et al., 2006, AJ, 132, 117
Goto T., 2006, MNRAS, 371, 769
Goto T., Utsumi Y., Hattori T., Miyazaki S., Yamauchi C., 2011, MNRAS, 415, L1
Gunn J. E., Peterson B. A., 1965, ApJ, 142, 1633
Kaiser N. et al., 2002, in Tyson J. A., Wolff S., eds, Proc. SPIE Conf. Ser. Vol. 4836, Survey and Other Telescope Technologies and Discoveries. SPIE, Bellingham, p. 154
Kaiser N. et al., 2010, in Stepp L. M., Gilmozzi R., Hall H. J., eds, Proc. SPIE Conf. Ser. Vol. 7733, Ground-based and Airborne Telescopes III. SPIE, Bellingham, p. 77330E
Kashikawa N. et al., 2002, PASJ, 54, 819
Komatsu E. et al., 2011, ApJS, 192, 18
Lawrence A. et al., 2007, MNRAS, 379, 1599
Li Y. et al., 2007, ApJ, 665, 187
McGreer I. D., Becker R. H., Helfand D. J., White R. L., 2006, ApJ, 652, 157
Matsuoka Y. et al., 2016, ApJ, 828, 26
Morganson E. et al., 2012, AJ, 143, 142
Mortlock D., 2016, in Mesinter A., ed., Astrophysics and Space Science Library, Vol. 423, Understanding the Epoch of Cosmic Reionization, Springer, Berlin, p. 187
Mortlock D. J. et al., 2011, Nature, 474, 616
Selsing J., Fynbo J. P. U., Christensen L., Krogager J.-K., 2016, A&A, 585, A87
Songaila A., 2004, AJ, 127, 2598
Stubbs C. W., Doherty P., Cramer C., Narayan G., Brown Y. J., Lykke K. R., Woodward J. T., Tonry J. L., 2010, ApJS, 191, 376
Tanaka T., Haiman Z., 2009, ApJ, 696, 1798
Tonry J. L. et al., 2012, ApJ, 750, 99
Vanden Berk D. E. et al., 2001, AJ, 122, 549
Venemans B. P. et al., 2013, ApJ, 779, 24
Venemans B. P. et al., 2015, ApJ, 801, L11
Wright E. L. et al., 2010, AJ, 140, 1868
Zhang S. N., Ji L., Kallman T. R., Yao Y. S., Froning C. S., Gu Q. S., Kriss G. A., 2015, MNRAS, 447, 2671

This paper has been typeset from a TEX/LATEX file prepared by the author.